# *Supplementary Information*

# Modelled sensitivity of Monte San Lorenzo ice cap, Patagonian Andes, to past and present climate

**Julian Martin[1,2], Bethan Davies[1,4]*, Richard Jones[3], Varyl Thorndycraft[1]**

[1]Centre for Quaternary Research, Department of Geography, Royal Holloway University of London, Egham, Surrey, TW20 0EX, UK

[2]Royal Geographical Society (with IBG), 1 Kensington Gore, London, SW7 2AR, UK

[3]School of Earth Atmosphere and Environment, Monash University, Clayton, Victoria, 3800, Australia.

[4]School of Geography, Politics and Sociology, Newcastle University, Newcastle upon Tyne, NE7 1RU

## 1 Supplementary Methods: Calculation of palaeo ELAs using GlaRe method

### 1.1 GlaRe-ELAs and Accumulation Area Balance Ratio (AABR)

In this study, we calculate the palaeo-equilibrium line altitude (ELA) of Calluqueo Glacier using the established Area-Altitude Balance Ratio (AABR) technique (Furbish and Andrews, 1984; Osmaston, 2005; Rea, 2009; Pellitero et al., 2015; Oien et al., 2021). Glacier ELAs are defined as the point at which annual accumulation and ablation are considered equal. Due to the relationship between temperature and precipitation at the glacier ELA (Ohmura et al., 1992), it is possible to obtain palaeoclimatic information from the ELA of a reconstructed palaeoglacier (Bendle and Glasser, 2012; Sagredo et al., 2014). If a record of past temperature is available, then a quantitative estimate of palaeoprecipitation can be derived.

The Area-Accumulation Balance Ratio (AABR) method takes account of glacier hypsometry and has been used extensively to reconstruct glacier and palaeo-glacier ELAs. The AABR method assumes that the mass balance/altitude curve consists of two linear segments, with different slopes above and below the glacier ELA (Osmaston, 2005). The balance ratio (BR) is the ratio of the slopes of the mass balance/altitude curve above and below the ELA (ibid). The AABR method therefore explicitly accounts for glacier hypsometry (distribution of glacier area with altitude) and the different accumulation and ablation gradients, and their control on glacier mass balance.

The choice of BR is a key control on the determination of glacier ELA. A balance ratio of 1 assumes that the accumulation and ablation gradients are equivalent, and is appropriate for polar regions (Rea, 2009). Balance ratios will be highest in tropical regions, where there is ablation all year and where ablation areas are correspondingly small. Rea (2009) found a global AABR of 1.75 ± 0.71, with balance ratios of mid-latitude maritime glaciers being 1.9 ± 0.81. More recently, Oien et al. (2021) have recommended a global AABR value of 1.56. However, our results found the resultant GlaRe-ELA to be the same with a balance ratio of both 1.5 and 1.75, and only 25 to 50 m lower with balance ratios of 2 to 2.5. The choice of balance ratio within this range therefore has little influence on the results, and we argue that our use of the 1.75 balance ratio is justified.

Freeware spreadsheets (Osmaston, 2005) and GIS tools (Pellitero et al., 2015, 2016) are now available to calculate the glacier ELA for a given balance ratio, and the GlaRe tool is used in this study.

## 1.2 GlaRe Palaeo ice-surface and ELA reconstruction

In this study, the GlaRe GIS tool for ArcGIS is used (Pellitero et al., 2016) to reconstruct palaeoglacier ice surface and glacier ELA. The model produces a two dimensional reconstruction of the glacier's flowline, assuming perfect plasticity rheology (Paterson, 1994), based upon the equation below for shear stress at the glacier's bed (Nye, 1952):

$$H = \frac{\tau}{(\rho g \sin \alpha)}$$

where $\tau$ is a uniform basal shear stress, $\rho$ is ice density and $\alpha$ is the ice surface slope, which is then interpolated to produce the 3D surface. This method also assumes the glacier is in equilibrium and is land-terminating. Once a palaeo-ice surface hasbeen reconstructed, this can be used as the input to an automatic calculation of the glacier ELA.

We used the GIS tool for ArcGIS developed by Pellitero et al. (2015, 2016) to produce AABR-derived ELAs, following Osmaston (2005), providing the advantage of rapid ELA calculation based upon the best estimate of the palaeo-ice surface. Balance ratios from 1.5to 2.5 were used to provide a range of possible ELAs, with a representative 'global' value of 1.75 selected for comparison to present day empirical data (Rea, 2009). We refer to ELAs reconstructed in this manner as GlaRe-ELAs.

## 1.3 Reconstruction of palaeotemperature and palaeoprecipitation at the GlaRe-ELA

The newly derived GlaRe-ELAs were combined with relative temperature offsets from the West Antarctic Ice Sheet (WAIS) Divide surface air temperature reconstruction (Cuffey et al., 2016) to calculate quantitative estimates of precipitation at the GlaRe-ELA for each phase of glacier stillstand (Ohmura et al., 1992). Changes in West Antarctic temperatures were synchronous with cryospheric changes in Patagonia's mid-latitudes (Bendle et al., 2019), with upwelling of warm deep water in the Southern Ocean a potential driver of warming across the mid and high- latitudes (Pedro et al., 2016). Although the quantitative transmission of this temperature change is unclear, the degree of temperature change across the ACR and the early Holocene as recorded in the chironomid records provides an indication that fluctuations in temperature are similar inthe Patagonian mid-latitudes observed in the WAIS Divide surface air temperature record (Cuffey et al., 2016). In light of an absence of coherent quantitative surface air temperature data from Patagonia across the LGIT and through the Holocene, this study therefore uses relative temperature offsets from present day from the WAIS Divide surface air temperature record (Cuffey et al., 2016) to obtain mean annual surface air temperature values at MSL for this period.

The temperature and precipitation at the glacier ELA has been linked directly via several empirical relationships (e.g., Ohmura et al., 1992). If summer mean temperatures at the glacier ELA can be calculated, then these empirical relationships can be used to derive quantitative estimates of palaeo-precipitation (Bendle and Glasser, 2012; Chandler and Lukas, 2017; Oien et al., 2021).

# 2 Supplementary Results: Evaluation of climatic forcing data

## 2.1 Temperature forcing

Two modelled climate gridded datasets, the Regional Atmospheric Climate Model (RACMO), version 2.3 for Patagonia (Lenaerts et al., 2014) and WorldClim2 (Fick and Hijmans, 2017), were investigated for their applicability to the study area and potential use to drive PISM spinup to present-day conditions. Average annual and monthly measured temperature and precipitation climate records from Lord Cochrane Aerodromo for the period 1970-2000 were compared with the respective modelled data from RACMO2.3 PAT5.5 and WorldClim2, alongside examinations of the datasets' modelled mean climate values for precipitation and temperature at Calluqueo Glacier, MSL (main manuscript), to establish which dataset is most appropriate to use to force PISM under present-day climate conditions. For surface air temperature, mean annual temperature point values, effective lapse rates, cosine yearly temperature cycles and dataset resolution are all assessed.

At Cochrane Aerodromo, both RACMO v.2.3 and WorldClim2 have temperature point values within 1°C of the instrumental data, although WorldClim2 is notably colder. However, with increased elevation at Calluqueo Glacier, RACMO2.3 modelled temperature is unrealistically cold compared with the meteorological data (see main manuscript) (Falaschi et al., 2013). The calculated lapse rates based upon RACMO2.3 point values (0.0072 °C $m^{-1}$ to 0.018 °C $m^{-1}$) also suggest that the modelled air temperature values from RACMO2.3 are unrealistically cold within the context of those observed across Patagonia. WorldClim2 produces temperature lapse rates (0.0051 °C $m^{-1}$ to 0.0056 °C $m^{-1}$) more akin to the observed regional values, including the lapse rate between San Lorenzo Sur and Lord Cochrane Aerodromo (0.0058 °C $m^{-1}$).

The annual temperature cycle is an important part of the mass balance scheme in PISM. In order to create seasonality within the mean annual temperature dataset, PISM has the facility to use a cosine yearly cycle temperature model, with the option of amplitude scaling ($A$). The annual temperature cycle is based upon mean annual and mean July temperatures and the year fraction since the previous July ($t$) (equation 1).

$$T(\text{time}) = T_{\text{mean annual}} + A(\text{time}) \cdot \left(T_{\text{mean July}} - T_{\text{mean annual}}\right) \cdot \cos(2\pi t) \qquad (1)$$

The fit to the annual temperature cycle examined between average monthly measured climate data at Lord Cochrane Aerodromo and the cosine yearly cycle climate model produced by PISM for this location based upon RACMO2.3 and WorldClim2 mean annual and mean July temperatures (Supplementary figure 1). Cosine yearly temperature cycles based upon data from RACMO2.3 and WorldClim2, without an amplitude scaling factor applied, do not produce the required amplitude of the measured annual temperature cycle (Supplementary figure 1A). The amplitude scaling factors which produce the best-fit annual temperature cycles to the measured cycle and are 1.55 and 1.25 for RACMO2.3 and WorldClim2 respectively (Supplementary figure 1A and B). Of these, WorldClim2 produces the closest fit to the measured instrumental climate cycle at Lord Cochrane Aerodromo (Supplementary figure 1D), producing a temperature cycle ranging from 1.5°C to 15.8°C (measured temperature cycle ranges from 1.8°C to 15.6°C, RACMO range from 1.5°C to 16.7°C).

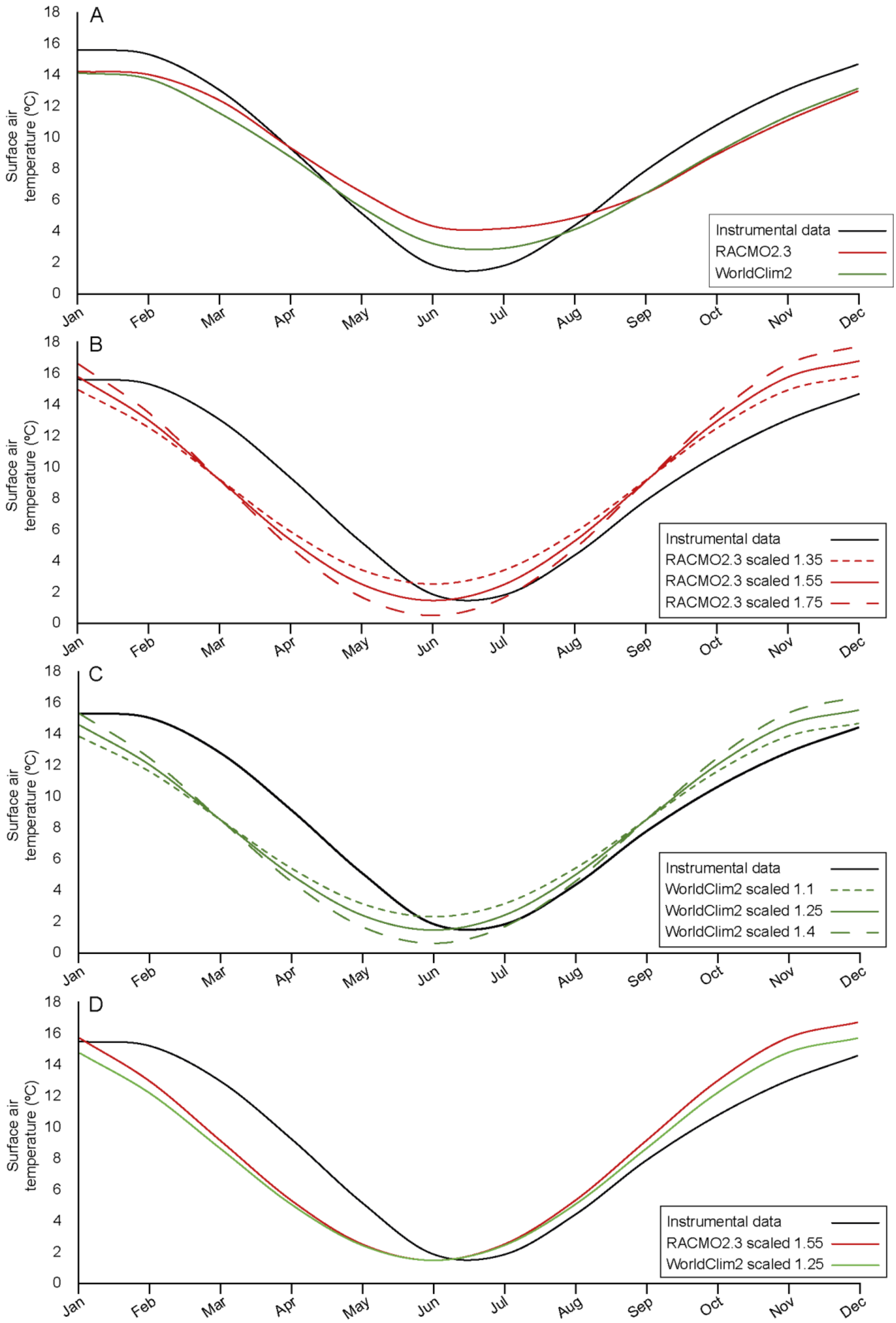


*Supplementary figure 1. Comparisons of annual temperature cycles from instrumental data from the Cochrane Aerodromo meteorological station and cosine curves for modelled climate data: A) with no amplitude scaling factors applied, B) RACMO2.3 data with amplitude scaling factors applied, C) WorldClim2 data with amplitude scaling factors applied and D) RACMO2.3 and*

*WorldClim2 data with 1.55 and 1.25 amplitude scaling respectively, representing the best fit scaled cosine curves with the meteorological station data.*

Finally, when modelling glaciers with steep long profiles (e.g. Calluqueo with a surface profile *ca* 20° gradient over a 7.75 km distance), it is important to take into account the resolution of climate dataset being used to initialise the model. This is important because elevation and in turn surface air temperature and precipitation change over a small horizontal distance. The higher resolution WorldClim2 dataset is better able to pick out temperature variations across and within the narrow valleys and highly varied mountain topography (Supplementary figure 2b,i). Notably for RACMO, the cold region over the summit of MSL extends further west than WorldClim2, into the lower elevations of Calluqueo valley, resulting in an unrealistically cold valley at low elevations (Supplementary figure 2a, e).

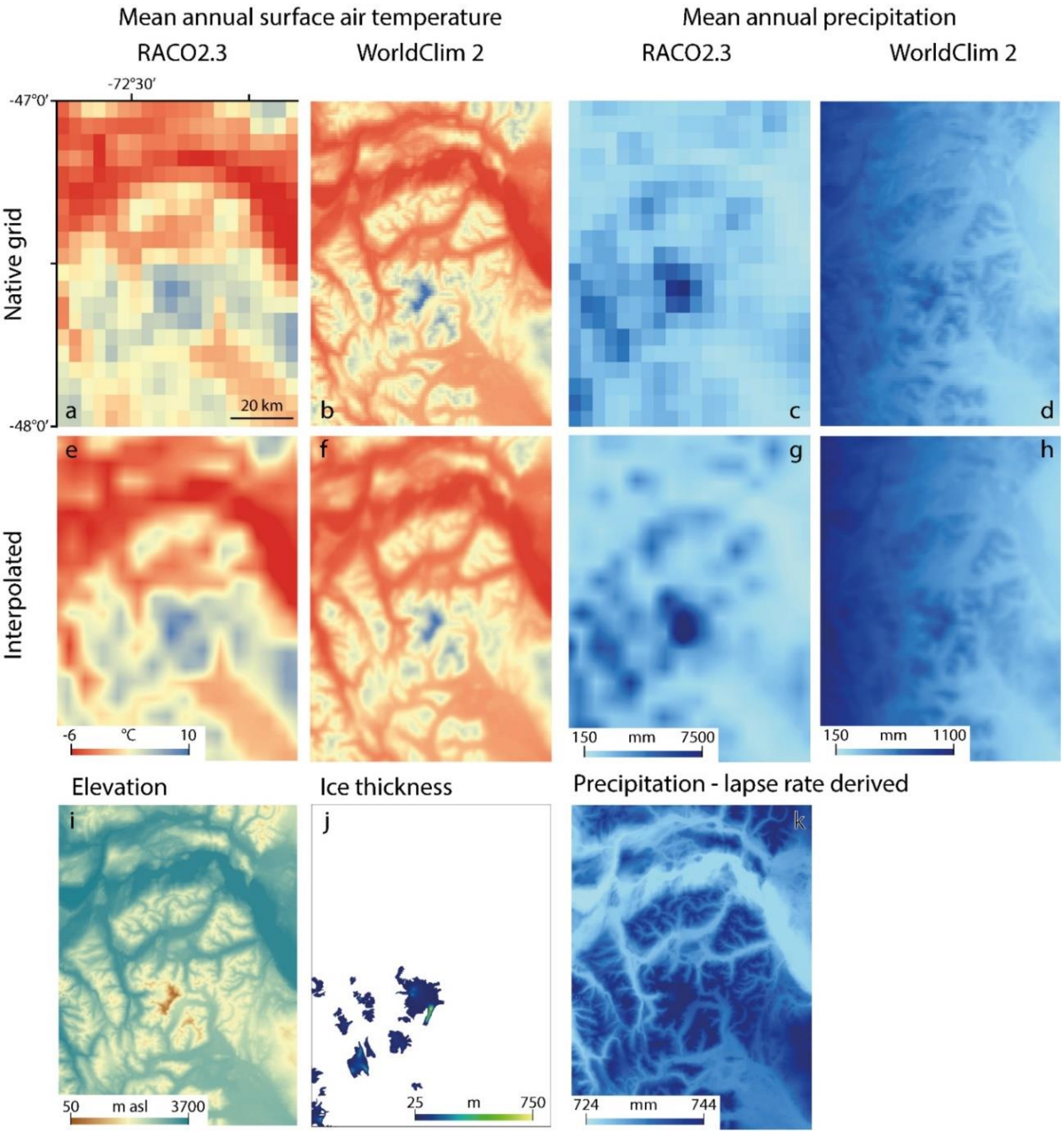


*Supplementary figure 2a to h) Gridded climate model data evaluated for use in PISM at both native resolution (RACMO2.3: 5.5 km, WorldClim2: 1 km) and bilinearly interpolated for input into PISM. i) ASTER GDEM j) modelled ice thickness data (Carrivick et al. 2016) and k) gridded precipitation dataset derived from Cochrane Aerodromo meteorological station precipitation data, an applied 1.35 mm/m precipitation lapse rate and ASTER GDEM (i).*

## 2.2 Precipitation forcing (Experiment A)

Initialising the ice cap model with WorldClim2 and RACMO2.3 precipitation data (Experiment A), alongside WorldClim2 temperature data and 'default' physical parameter values produced model simulations with too little and too much ice respectively in comparison to present-day ice extent (Supplementary figure 3). Both RACMO2.3 and WorldClim2 precipitation datasets were therefore considered unrepresentative of precipitation at Calluqueo Glacier, with precipitation being too high and too low respectively. Although the spatial distribution of RACMO2.3 precipitation data across the catchment appears reasonable (Supplementary Figure 2g), scaling down precipitation across the catchment to create a more realistic value at MSL would in turn create unrealistically arid lower-altitude valleys.

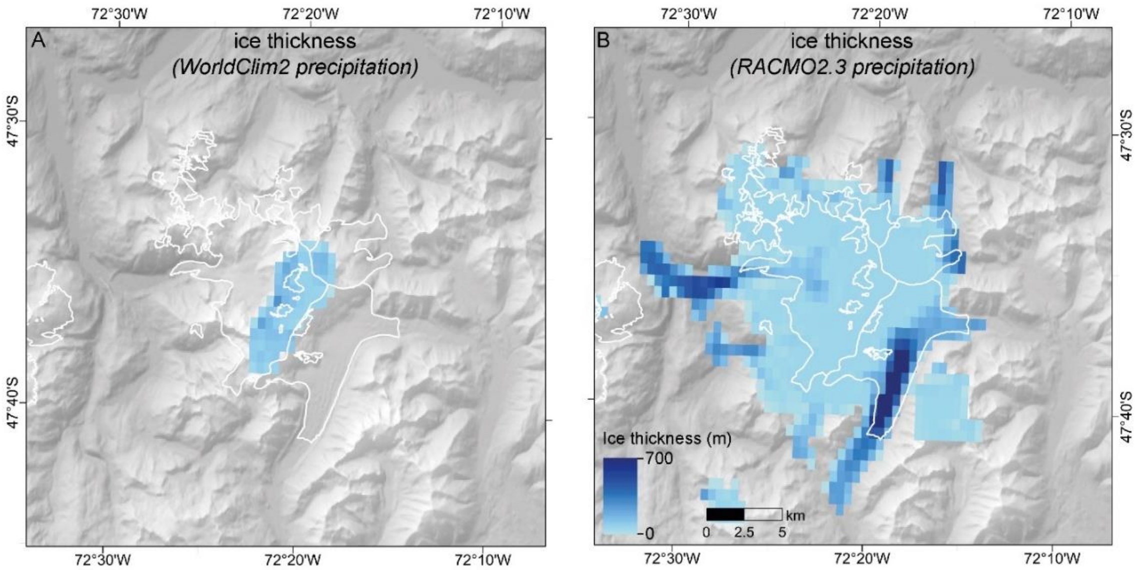


*Supplementary figure 3. Modelled ice thickness when initialised with precipitation from the WorldClim2 (A) and RACMO2.3 (B) modelled climate datasets.*

## 2.3 Supplementary results: Sensitivity experiments

### 2.3.1 Ice rheology and bed strength (Experiment C)

Changing the basal shear strength parameter within PISM acts as a control on ice thickness and extent (Supplementary figure 4). Although it would be expected that a lower basal shear strength simulating a weaker substrate would lead to a longer and thinner glacier profile (Golledge et al., 2012), the simulations show that the lowest strength value tested (25 kPa) produces the shortest simulation of Calluqueo Glacier. As the model simulations evolve, they show initial rapid glacier advance beyond the final equilibrium position, before recession and stabilisation (Supplementary Figure 4). Calluqueo Glacier advances rapidly at the start of the simulation due to an initial net positive mass balance. The simulation with a basal shear strength of 25 kPa advanced furthest to a maximum distance *ca* 6.25 km down valley of the present-day glacier terminus, whereas the 50 kPa simulation advanced only *ca* 5.25 km ahead of the present-day terminus, but produced a thicker glacier. This difference is a product of the basal shear strength, where low bed strength initially leads to a longer and thinner glacier, with the ice able to flow down valley more readily. Excess ablation then leads to retreat of the terminus back to its equilibrium position (Cuffey and Paterson, 2010). Having established a greater thickness of ice, the simulation with the stronger bed maintains its length and thickness during the ablation phase better than the thinner glacier formed over the weaker bed.

It is generally thought that in scenarios of sudden decreases in basal shear strength, e.g. due to the input of meltwater and increase in basal water pressure, the accumulation zone thins as a result of increased mass flux down the glacier. This thinning is propagated down the glacier, increasing its length and reducing its thickness (Fountain et al., 2004; Cuffey and Paterson, 2010). This evolution of the ice thickness is replicated in our study, suggesting that increasing basal meltwater could contribute to dynamic thinning.

The simulations show that implementing a flow enhancement factor of 3 produces a longer glacier profile, as would be expected for simulating ‘softer’ ice which deforms more easily by internal shear (Ritz et al., 1996; Parizek and Alley, 2004). Although not shown on Supplementary figure 4, implementing an enhancement factor of 5 does not change the glacier’s long profile when modelled at a 250 m horizontal resolution.

For the remaining sensitivity experiments, the SIA enhancement factor and basal yield strength were set as mid-range values (3 and 35 kPa respectively; Table 3 in main manuscript), in line with those found to best fit a similar mountain valley glacier setting (Golledge et al., 2012) and within the range observed globally (Table 3 in main manuscript).

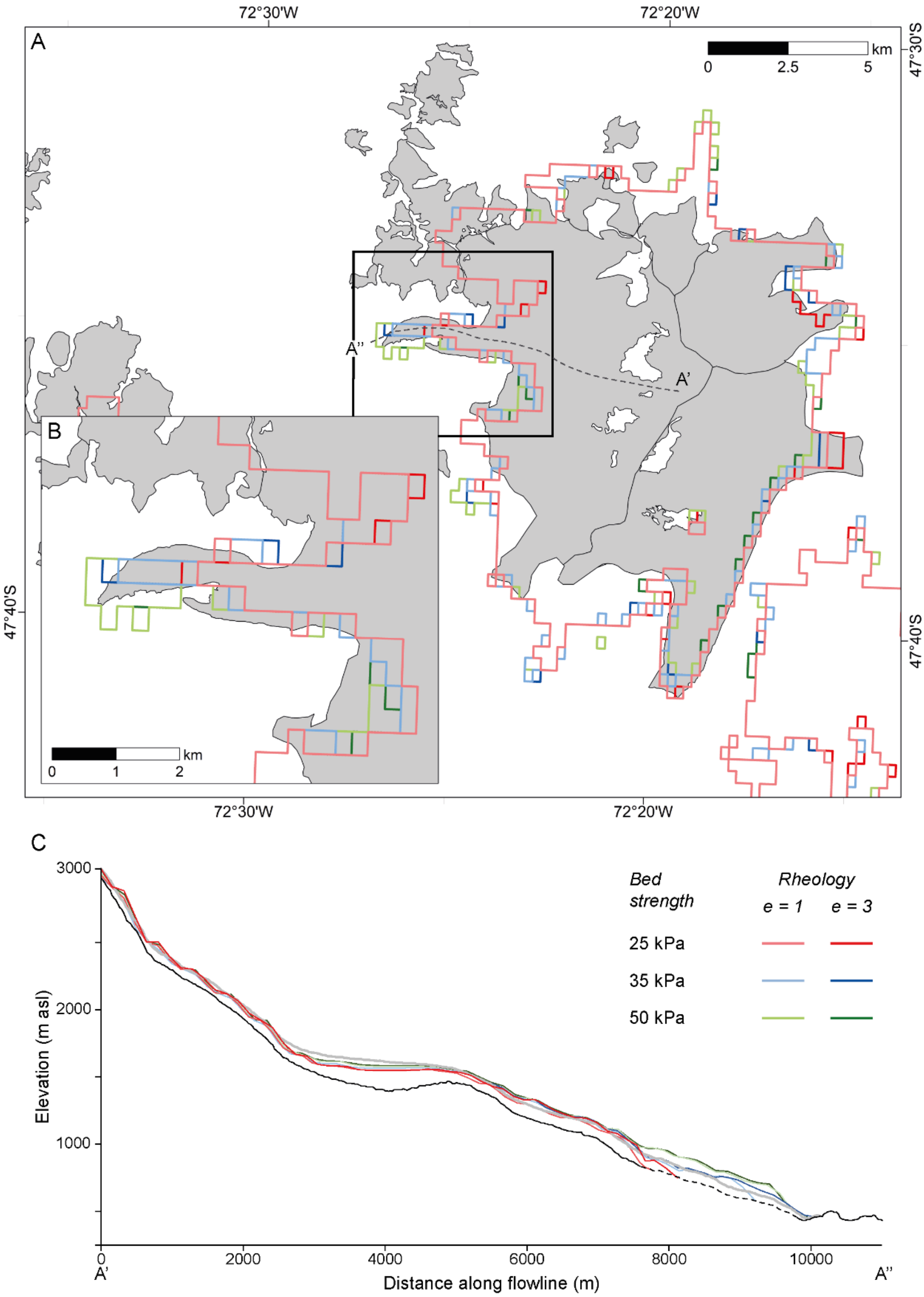


*Supplementary figure 4. Simulated ice cap extents at MSL under different basal shear strengths and flow enhancement factors. Coloured lines correspond to legend in Panel C. B) Inset map focusing on Calluqueo Glacier. C) Long profile of Calluqueo Glacier, corresponding to the profile A' A" in Panel A. Note the modelled bedrock is unable to resolve a realistic bed at the lower section of the glacier, indicating an ice thickness of zero. The bed geometry is therefore estimated and shown by a dotted black line.*

### 2.3.2 Positive degree day melt factors (Experiment D)

A series of degree-day factors for snow and ice have been measured in southern Patagonia. They range from 3.5 mm w.e. snow and 7 to 7.6 mm w.e. ice at Gran Campo Nevado (Möller et al., 2007; Schneider et al., 2007) to 2.7 to 7.6 at Perito Moreno Glacier (Stuefer et al., 2007) (Supplementary Table 1).

*Supplementary Table 1. Measured degree day factors in mm w.e. d-1 °C, in part after Hock et al. (2003).*

| **Location** | **Degree day factor (snow)** | **Degree day factor (ice)** | **Reference** |
|---|---|---|---|
| Chico Glacier | 4 | 6.5 | Rivera (2004) |
| Perito Moreno Glacier | | 2.7 to 4.3 | Stuefer et al. (2007) |
| | | 7.1 | Takeuchi et al. (1996) |
| Franz Josef Glacier (NZ) | 3 | 6 | Woo and Fitzharris, (1992); Bravo et al., (2015) |
| | 4.6 | 7.2 | Anderson B. et al., (2006) |
| Campo Nevado Ice Cap | | 7.6 | Schneider et al. (2007) |
| Aletschgletscher (Switzerland) | 5.3 | | |
| John Evans Glacier (Canada) | 2.7 to 5.5 | 5.5 to 7.6 | Arendt and Sharp, (1999) |

To assess the sensitivity of modelled glaciers at MSL to changes in degree-day factor values, a range in mm water equivalent (mm w.e.) of 1.5, 3 and 8 for snow and 3, 8 and 16 for ice were chosen to reflect the range empirically observed in Patagonia and mountain glacier settings globally (Supplementary Table 1) (Lang, 1986; Takeuchi et al., 1996; Arendt and Sharp, 1999; Hock, 2003; Anderson B. et al., 2006; Möller et al., 2007; Schneider et al., 2007) and in line with previous mountain glacier modelling sensitivity studies (e.g. Golledge et al., 2012; Jouvet et al., 2017; Yan et al., 2018).

Setting low degree-day factors within PISM's positive degree-day model produces a greater ice extent, while high degree-day factors lead to a smaller ice extent (Supplementary figure 5). When using low degree-day factors (e.g. values of 3 and 1.5 for ice and snow respectively), outlet glaciers flowing into low altitude valleys experience less melt for the same surface air temperature as when higher degree day factors are used. This results in ice maintained in the low altitude valleys. More specifically, simulations show that for the same increase in degree-day factor for snow and ice, an increase in ice melt causes a greater reduction in ice extent and volume than the same increase in snow melt (Supplementary figure 5).

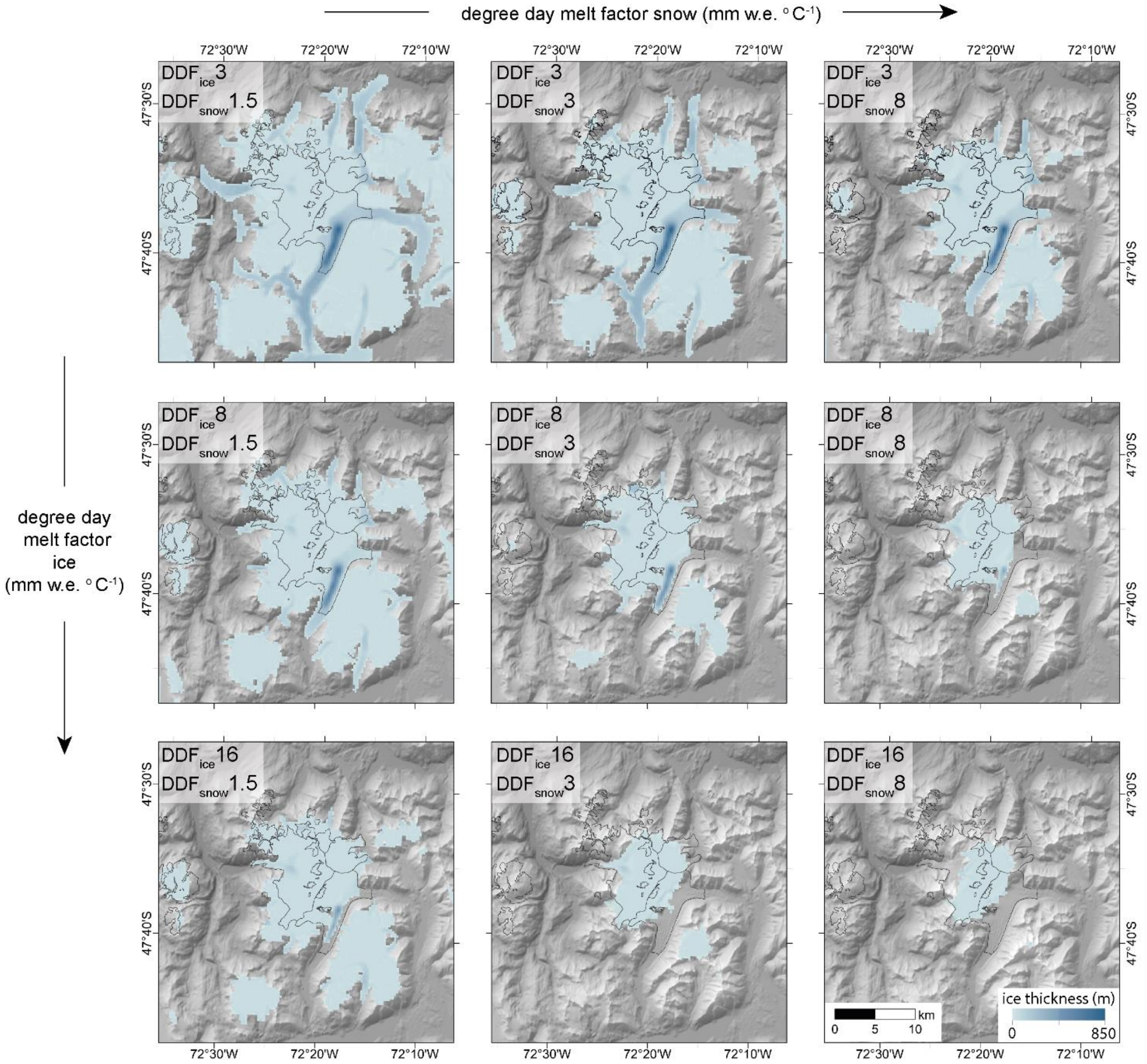


*Supplementary figure 5. Model simulations of the MSL ice cap under the implementation of different degree-day factors within PISM's positive degree-day model.*

# References


Anderson B., Lawson W., Owens I., and Goodsell, B. (2006). Past and future mass balance of Ka Roimata o Hine Hukatere (Franz Josef Glacier). *J. Glaciol.* 52, 597–607.

Arendt, A., and Sharp, M. (1999). Energy balance measurements on a Canadian high Arctic glacier and their implications for mass balance modelling. *IAHS Publ.*, 165–172.

Bendle, J. M., and Glasser, N. F. (2012). Palaeoclimatic reconstruction from Lateglacial (Younger Dryas Chronozone) cirque glaciers in Snowdonia, North Wales. *Proc. Geol. Assoc.* 123, 130–145.

Bendle, J. M., Palmer, A. P., Thorndycraft, V. R., and Matthews, I. P. (2019). Phased Patagonian Ice Sheet response to Southern Hemisphere atmospheric and oceanic warming between 18 and

17 ka. *Sci. Rep.* 9, 4133. doi:10.1038/s41598-019-39750-w.

Bravo, C., Rojas, M., Anderson, B. M., Mackintosh, A. N., Sagredo, E., and Moreno, P. I. (2015). Modelled glacier equilibrium line altitudes during the mid-Holocene in the southern mid-latitudes. *Clim. Past* 11, 1575–1586.

Chandler, B. M. P., and Lukas, S. (2017). Reconstruction of Loch Lomond Stadial (Younger Dryas) glaciers on Ben More Coigach, north-west Scotland, and implications for reconstructing palaeoclimate using small ice masses. *J. Quat. Sci.* 32, 475–492.

Cuffey, K. M., Clow, G. D., Steig, E. J., Buizert, C., Fudge, T. J., Koutnik, M., et al. (2016). Deglacial temperature history of West Antarctica. *Proc. Natl. Acad. Sci.* 113, 14249–14254.

Cuffey, K. M., and Paterson, W. S. B. (2010). *The Physics of Glaciers, 4th edition*. Academic Press.

Falaschi, D., Bravo, C., Masiokas, M., Villalba, R., and Rivera, A. (2013). delete this one. *Arctic, Antarct. Alp. Res.* 45, 19–28. doi:http://dx.doi.org/10.1657/1938-4246-45.1.19.

Fick, S. E., and Hijmans, R. J. (2017). WorldClim 2: new 1-km spatial resolution climate surfaces for global land areas. *Int. J. Climatol.* 37, 4302–4315.

Fountain, A. G., Neumann, T. A., Glenn, P. L., and Chinn, T. (2004). Can climate warming induce glacier advance in Taylor Valley, Antarctica? *J. Glaciol.* 50, 556–564. doi:10.3189/172756504781829701.

Furbish, D. J., and Andrews, J. T. (1984). The use of hypsometry to indicate long-term stability and response of valley glaciers to changes in mass transfer. *J. Glaciol.* 30, 199–211.

Golledge, N. R., Mackintosh, A. N. N., Anderson, B. M. M., Buckley, K. M. M., Doughty, A. M. M., Barrell, D. J. A. J. A., et al. (2012). Last Glacial Maximum climate in New Zealand inferred from a modelled Southern Alps icefield. *Quat. Sci. Rev.* 46, 30–45. doi:10.1016/j.quascirev.2012.05.004.

Hock, R. (2003). Temperature index melt modelling in mountain areas. *J. Hydrol.* 282, 104–115. doi:http://dx.doi.org/10.1016/S0022-1694(03)00257-9.

Jouvet, G., Seguinot, J., Ivy-Ochs, S., and Funk, M. (2017). Modelling the diversion of erratic boulders by the Valais Glacier during the last glacial maximum. *J. Glaciol.* 63, 487–498.

Lang, H. (1986). “Forecasting Meltwater Runoff from Snow-Covered Areas and from Glacier Basins,” in (Springer, Dordrecht), 99–127. doi:10.1007/978-94-009-4536-4_5.

Lenaerts, J. T. M., Van Den Broeke, M. R., van Wessem, J. M., van de Berg, W. J., van Meijgaard, E., van Ulft, L. H., et al. (2014). Extreme precipitation and climate gradients in Patagonia revealed by high-resolution regional atmospheric climate modeling. *J. Clim.* 27, 4607–4621.

Möller, M., Schneider, C., and Kilian, R. (2007). Glacier change and climate forcing in recent decades at Gran Campo Nevado, southernmost Patagonia. *Ann. Glaciol.* 46, 136–144. Available at: http://www.ingentaconnect.com/content/igsoc/agl/2007/00000046/00000001/art00021 http://dx.doi.org/10.3189/172756407782871530.

Nye, J. F. (1952). The mechanics of glacier flow. *J. Glaciol.* 2, 82–93.

Ohmura, A., Kasser, P., and Funk, M. (1992). Climate at the equilibrium line of glaciers. *J. Glaciol.* 38, 397–411.

Oien, R. P., Rea, B. R., Spagnolo, M., Barr, I. D., and Bingham, R. G. (2021). Testing the area–altitude balance ratio (AABR) and accumulation–area ratio (AAR) methods of calculating glacier equilibrium-line altitudes. *J. Glaciol.*, 1–12. doi:DOI: 10.1017/jog.2021.100.

Osmaston, H. (2005). Estimates of glacier equilibrium line altitudes by the Area×Altitude, the Area×Altitude Balance Ratio and the Area×Altitude Balance Index methods and their validation. *Quat. Int.* 138–139, 22–31. Available at: http://www.sciencedirect.com/science/article/B6VGS-4G4N5T8-1/2/b605e874411c5efe77f7615693584c68.

Parizek, B. R., and Alley, R. B. (2004). Ice thickness and isostatic imbalances in the Ross Embayment, West Antarctica: model results. *Glob. Planet. Change* 42, 265–278. doi:10.1016/J.GLOPLACHA.2003.09.005.

Paterson, W. S. B. (1994). The physics of glaciers, 480 pp.

Pedro, J. B., Bostock, H. C., Bitz, C. M., He, F., Vandergoes, M. J., Steig, E. J., et al. (2016). The spatial extent and dynamics of the Antarctic Cold Reversal. *Nat. Geosci.* 9, 51–55.

Pellitero, R., Rea, B. R., Spagnolo, M., Bakke, J., Hughes, P., Ivy-Ochs, S., et al. (2015). A GIS tool for automatic calculation of glacier equilibrium-line altitudes. *Comput. Geosci.* 82, 55–62. doi:https://doi.org/10.1016/j.cageo.2015.05.005.

Pellitero, R., Rea, B. R., Spagnolo, M., Bakke, J., Ivy-Ochs, S., Frew, C. R., et al. (2016). GlaRe, a GIS tool to reconstruct the 3D surface of palaeoglaciers. *Comput. Geosci.* 94, 77–85.

Rea, B. R. (2009). Defining modern day Area-Altitude Balance Ratios (AABRs) and their use in glacier-climate reconstructions. *Quat. Sci. Rev.* 28, 237–248. doi:http://dx.doi.org/10.1016/j.quascirev.2008.10.011.

Ritz, C., Fabre, A., and Letréguilly, A. (1996). Sensitivity of a Greenland ice sheet model to ice flow and ablation parameters: consequences for the evolution through the last climatic cycle. *Clim. Dyn.* 13, 11–23. doi:10.1007/s003820050149.

Rivera, A. (2004). Mass balance investigations at Glaciar Chico, Southern Patagonia Icefield, Chile. *South. Patagon. Icefield, Chile.*

Sagredo, E. A., Rupper, S., and Lowell, T. V (2014). Sensitivities of the equilibrium line altitude to temperature and precipitation changes along the Andes. *Quat. Res.* 81, 355–366. doi:http://dx.doi.org/10.1016/j.yqres.2014.01.008.

Schneider, C., Kilian, R., and Glaser, M. (2007). Energy balance in the ablation zone during the summer season at the Gran Campo Nevado Ice Cap in the Southern Andes. *Glob. Planet. Change* 59, 175–188. doi:10.1016/j.gloplacha.2006.11.033.

Stuefer, M., Rott, H., and Skvarca, P. (2007). Glaciar Perito Moreno, Patagonia: climate sensitivities and glacier characteristics preceding the 2003/04 and 2005/06 damming events. *J. Glaciol.* 53, 3–16. doi:10.3189/172756507781833848.

Takeuchi, Y., Naruse, R., and Skvarca, P. (1996). Annual air-temperature measurement and ablation estimate at Moreno Glacier, Patagonia. *Bull. glacier Res.* 14, 23–28.

Woo, M., and Fitzharris, B. B. (1992). Reconstruction of mass balance variations for Franz Josef Glacier, New Zealand, 1913 to 1989. *Arct. Alp. Res.* 24, 281–290.

Yan, Q., Owen, L. A., Wang, H., and Zhang, Z. (2018). Climate Constraints on Glaciation Over High-Mountain Asia During the Last Glacial Maximum. *Geophys. Res. Lett.* 45, 9024–9033. doi:https://doi.org/10.1029/2018GL079168.